Electrical Transport and Photoemission Experiments of Alkylphosphonate Monolayers on GaAs

ARTICLE *in* THE JOURNAL OF PHYSICAL CHEMISTRY C · FEBRUARY 2009

Impact Factor: 4.77 · DOI: 10.1021/jp808086d

Electrical Transport and Photoemission Experiments of Alkylphosphonate Monolayers on GaAs

Hagay Shpaisman,[†] Eric Salomon,[§] Guy Nesher,[†] Ayelet Vilan,[†,‡] Hagai Cohen,[‡] Antoine Kahn,[§] and David Cahen*[,†]

Department of Materials & Interfaces, and Department of Chemical Support, Weizmann Institute of Science, Rehovoth, Israel 76100 and Department of Electrical Engineering, Princeton University, Princeton, New Jersey

Received: September 11, 2008; Revised Manuscript Received: December 22, 2008

We report on electronic transport measurements through dense monolayers of $CH_3(CH_2)_nPO_3H_2$ molecules of varying chain lengths, with a strong and stable bond through the phosphonic acid end group to a <100> GaAs surface and a Hg top contact. The monolayers maintain their high quality during and after the electrical measurements. Analyses of the electronic transport measurements of junctions, and of UV and inverse photoemission spectroscopy data on band alignments of free surfaces, yield insight about the electrical transport mechanism. Transport characteristics for n-GaAs junctions at low forward bias are identical for different chain lengths, a strong indication of high-quality monolayers. Tunneling barrier and carrier effective mass values for n- and p-GaAs samples were deduced from the transport data. In this way we find a tunneling barrier for n-GaAs of 1.3 eV, while UPS data for the lowest unoccupied system orbital (LUSO) point to a 2.4 eV barrier. This discrepancy can be understood by invoking states, closer to the Fermi level than the LUSO state, that contribute to charge transport. Such states lead to a manifold of transitions, each having a different probability, both because of differences in the tunnel barrier and because of differences in density of these interface-induced states; i.e., the single barrier, deduced from $J-V$ measurements, is an effective value only.

1. Introduction

Adsorbing molecules on the surface of semiconductors can change the semiconductors' electronic properties dramatically. It has been shown that molecular properties can be coupled with the electrical and optical properties of a variety of semiconductors.[1,2] In addition to molecular adsorption on II−VI semiconductors and Si/Si oxide, molecular modification of GaAs has received significant attention, notwithstanding the unstable character of the free, unmodified GaAs surface in ambient.[3] GaAs-based devices have some unique applications,[4−6] and while the instability of GaAs surfaces makes it difficult to achieve reproducible free surface properties, molecular modification via strong chemical bonding provides significant passivation of the resulting surface. Molecular modifications have been done, in order of increasing binding strength, with thiol[7−10] and carboxylic[11,12] functional groups, and lately with phosphates[13] and phosphonates.[14]

One of our major research goals is to understand electrical transport across organic molecules, particularly saturated ones (see below). Such electrical transport is studied widely using metal/molecule(s)/metal junctions. Replacing one of the metals by a semiconductor introduces, on one hand, some complications in the interpretation of the transport mechanisms, but on the other hand allows changing the work function of the electrode without, to a first approximation, changing the nature of the molecule/semiconductor chemical bond. In addition, it becomes possible to study the importance of the polar character of the interface in ways well beyond what is possible in the metal/molecule/metal junctions.

Studies of semiconductor/molecules/metal junctions using Si[15,16] and GaAs[8,14,17−19] have been previously reported and, especially the work of Nesher et al.,[14] serve as a basis for this work. We note that one needs to be careful when measuring electrical transport on chemically bound monolayers, as the measurement can lead to dislodging the molecules from the surface. Thus, in our earlier work with S-bound molecules to GaAs, we found that there was only reproducibility between the first transport measurements for each (Hg) contact to the molecules, as the measurement itself led to changes in the junction. That finding led us to use the much more robust phosphonate binding group.

Although conjugated molecules, with a relatively small energy gap between highest occupied and lowest unoccupied molecular orbitals (HOMO and LUMO, respectively) and an obvious path for electronic conduction, are attractive candidates for molecular electronics, we focus here on large-gap saturated molecules (namely alkyls). The reasons are the following:

- Most molecules are not conjugated, and, thus, conclusions drawn from work with conjugated molecules are not necessarily widely applicable.
- These are simple molecules, in terms of composition and structure, that can easily be obtained as series with systematically varying properties (length, dipole).
- Last but not least, they can form densely packed monolayers.

The last two aspects are crucial to help reveal fundamental mechanisms of electronic transport across molecules with localized electronic states.

While choosing a properly doped semiconductor, onto which the molecules are adsorbed, establishes and helps control one of the electronic contacts, special care should be taken with the other electrical contact required for measuring current transport.

* To whom correspondence should be addressed. E-mail: david.cahen@weizmann.ac.il.
[†] Department of Materials & Interfaces, Weizmann Institute of Science.
[‡] Department of Chemical Support, Weizmann Institute of Science.
[§] Department of Electrical Engineering.

10.1021/jp808086d CCC: $40.75
Published on Web 02/03/2009

Conventional deposition of a metal as contact on the side of the molecules that is not bound to the semiconductor surface can easily damage the organic molecules.[20] Gentle, nondestructive, and noninvasive methods should be used to make sure that the electronic carriers indeed pass through the molecules, and not through pinholes in the layer. Several methods such as liftoff float-on (LOFO),[21] nanotransfer printing,[22] and indirect metal evaporation[23] on molecules have been devised. A simpler method is using a liquid metal, preferably one that does not easily oxidize, i.e., mercury.[24,25] The very high surface tension of liquid metals limits their ability to penetrate into monolayer defects, thus avoiding shorting through pinholes[26] and leading to excellent reproducibility.

Here we use a series of relatively well-defined monolayers, bound to the GaAs surface via a phosphonic acid group. This group creates a strong bond that is stable also during electrical measurements. The series is constructed of $CH_3(CH_2)_nPO_3H_2$ molecules of different chain lengths ($n = 7, 9, 11, 13, 15, 17$; to be referred to as C8, C10, C12, C14, C16, and C18, respectively). We first describe the quality of the monolayers that are formed. We then show what insights can be gained into the electrical transport mechanism and energy level and band alignment from current−voltage and UV and inverse photoemission spectroscopic measurements.

2. Experimental Section

Chemicals. *n*-Octylphosphonic acid (>98%), *n*-decylphosphonic acid (>98%), *n*-dodecylphosphonic acid (>99%), *n*-tetradecylphosphonic acid (>97%), *n*-hexadecylphosphonic acid (>98%), and *n*-octadecylphosphonic acid (>97%) were purchased from Poly Carbon Industries Inc. Extra pure Hg (7 N; Fluka) was used. InGa was either purchased from Sigma and used as received or prepared as an In/Ga mixture (1/3 ratio). In the latter case, the mixture was heated until it melted and then cooled to create an eutectic mixture. Solvents were reagent grade or better, purchased from Merck or Bio-Laboratory. All chemicals were used without further purification.

Sample Preparation. <100> oriented, $1.4-2.0 \times 10^{18}$ cm^{-3} n-doped (Si) GaAs wafers and $8.9-9.6 \times 10^{18}$ cm^{-3} p-doped (Zn) ones were purchased from AXT (CA, U.S.). The GaAs substrates were first cleaned sequentially in an ultrasonic bath with isopropanol, acetone, and methanol (10 min for each solvent). Then they were treated by ozone oxidation for 25 min in a UVOCS apparatus (model T10 × 10). Finally, the oxide was chemically removed by a sequential process of dipping the samples for 5 s in a 2% hydrofluoric acid solution, rinsing in MilliQ water, dipping for 30 s in dilute NH_4OH (1:9) solution, and rinsing in MilliQ water again.[27,28] After drying under a stream of dry N_2, the samples were introduced immediately in the adsorption solution (1 mM in tetrahydrofuran (THF)). The solution was heated for 5 min to 50 °C and placed in a N_2 atmosphere for 3 min. The samples were then transferred to a desiccator for one night. After the adsorption process and before the measurements, samples were rinsed again with methanol. Next, the samples were immersed in an ultrasonic bath of ethyl acetate for 3 min. Finally, they were dipped in boiling dichloromethane for 3 min.

Ellipsometry. Molecular layer thickness was deduced from ellipsometric measurements, using a spectroscopic ellipsometer with a spectral range from 370 to 1000 nm (J. A. Woollam Co. Inc., model M 2000V). Data were fit using WVase32 software, using a Cauchy model for the top organic layer with $a = 1.45$, $b = 0.01$, $c = 0$.

Contact Angle Measurements (CA). Static contact angle measurements were performed with an automated goniometer (Ramé-Hart, Model-100). Approximately 4 μL of deionized water (Millipore Inc.) was deposited onto the sample using a microsyringe (advancing drop method). Measurements were recorded immediately after deposition.

Fourier Transform Infrared (FTIR). Measurements were performed on a BRUKER, EQUINOX-55 in the transmission mode, using a liquid nitrogen cooled mercury cadmium telluride (MCT) detector. The spectra were corrected for background by subtracting a reference spectrum obtained from a freshly cleaned and etched GaAs sample.

Contact Potential Difference (CPD). We used a home-built apparatus to measure the work function, based on a commercial Besocke Delta Phi Kelvin probe. In this system, a vibrating Au grid is used as a reference probe.[29,30] The band bending was estimated by measuring the difference between the CPD with the sample under strong illumination (~0.5 W/cm^2) where the bands are almost flat, and for the sample in the dark. The measurements were done inside a Faraday cage, in order to minimize electrical noise, within a glovebox under N_2 atmosphere.

X-ray Photoelectron Spectroscopy (XPS). Measurements were performed at the Weizmann Institute on a Kratos Analytical AXIS-HS instrument, using a monochromatized Al Kα (1486.6 eV) source at a relatively low power, 75 W, and detection pass energy of 20 eV. Composition and thickness analysis were deduced from the O1s, C1s, Ga3d, As3d, and P2p lines. Ga2p and As2p lines were analyzed as well to gain insight in the nature of the oxide species. Curve fitting with Gaussian−Lorentzian line shapes was applied. Beam-induced damage was studied by performing repeated scans on a fixed spot and then selecting fresh spots for measurement at optimal conditions.

Our XPS thickness analysis assumes a model structure with a homogeneous organic top layer of thickness d_{org} and a thin interfacial layer, of thickness d_{inorg}, where oxide species[1] are incorporated between the organic monolayer and the GaAs substrate, or embedded close to the interface, between the monolayer molecules. Attenuation of the emitted photoelectrons is accounted for by an inelastic mean free path (IMFP) parameter of 33 Å for the organic layer and 25 Å for the inorganic layer,[31,32] neglecting their kinetic energy dependence across the low binding energy range, up to 550 eV.[33] Organic (defined as the alkyl chain with the phosphonic acid head group) and inorganic layer thicknesses are given by the following expressions

$$d_{org} = \lambda^{org} \sin\theta \cdot \ln\left(\frac{[C]+[P]+[O^{org}]}{[Ga]+[As]+[O^{inorg}]}+1\right) \quad (1)$$

$$d_{inorg} = \lambda^{inorg} \sin\theta \cdot \ln\left(\frac{inorganic\_overlayer}{[Ga^{sub}]+[As^{sub}]}+1\right) \quad (2)$$

where λ^{org} and λ^{inorg} are the IMFP values of the organic and inorganic matrices, respectively. Atomic concentrations are given within square brackets. We assume $[O^{org}] = 3[P]$ and thus $[O^{inorg}] = [O] - [O^{org}]$. The identity of the inorganic overlayer is discussed below. θ is the takeoff emission angle with respect to the surface plane. Ga^{sub} and As^{sub} are the Ga and As signals of the (nonoxidized) wafer. In addition to the above approximations, error in the thickness analysis is introduced by the angular broadening of the magnetic lens in the detection system, estimated to have a small effect at 90° and, however, up to 20% at 30°.

Ultraviolet Photoelectron Spectroscopy (UPS). Filled valence states of the alkylphosphonate-covered GaAs surfaces were

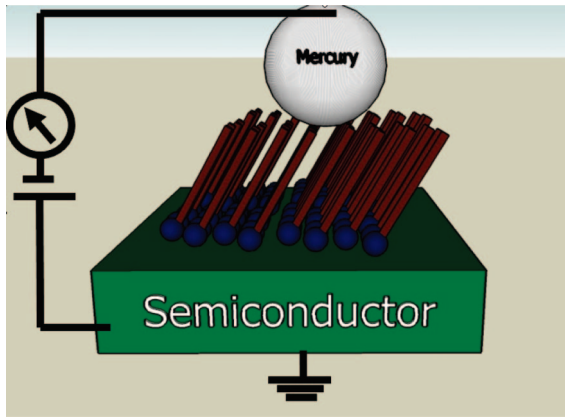

Figure 1. Schematic illustration of the GaAs/monolayer//Hg junction and the current transport-measuring system. Monolayer is very much enlarged for the sake of clarity.

measured by direct photoemission spectroscopy at Princeton University. Valence band spectra and vacuum level positions were measured by UPS, using He II (40.81 eV) excitation. Since the UPS signal of the GaAs is strongly attenuated after molecular adsorption, it is difficult to determine whether or not the organic layer induces band bending. Therefore, UPS was also complemented by *in situ* XPS in Princeton, to evaluate the evolution of the Ga and As core levels with respect to the Fermi level and, thus, the band bending in the semiconductor with the molecular overlayer. Both Al Kα (1486.6 eV) and Zr Mζ (151.4 eV) emission lines were used to get different surface sensitivities. The Ga and As 3d core levels and valence band positions were measured in order to establish the band bending. The binding energies given correspond to the positions of the centers of the Gaussian peaks used for decomposition. The position of the Fermi level of the spectrometer was measured via UPS on a clean Au substrate. The overall instrumental resolution in UPS, measured from the Au Fermi step, was 150 meV.

Inverse Photoemission Spectroscopy (IPES). Unoccupied states of the alkylphosphonate-covered GaAs surfaces were measured via IPES, performed in the isochromat mode using a fixed-energy photon detector and a low-energy electron gun.[34,35] The overall IPES instrumental resolution, estimated from the width of the Fermi edge measured on Ta, is 450 meV. The primary electron current density was held below 1 μA/cm^2.

Current Density−Voltage ($J-V$) Measurement. The Hg drop setup has been described in previous work[18] and is schematically shown in Figure 1. Current density−voltage characteristics were collected in the voltage scan mode, using a Keithley 6430 picoammeter. The bias polarity convention is that the voltage is positive for junctions on p-type samples as the Hg drop (top contact) is negatively polarized and vice versa for n-type samples (voltage is positive for positively polarized Hg contact). Results are independent of the scan rate, and we found no detectable deterioration of the monolayer over multiple scans. The optical cross section of the Hg droplet with the substrate was taken as the formal contact area, to convert measured currents into formal current densities. Every $J-V$ curve is an average of several independent junctions made on 3 samples that were prepared separately on different occasions, yielding at least 10 measurements (except for the C8 junction, where a total of 6 measurements from 2 different samples was used; the shorter the alkyl chain, the more difficult the preparation of high-quality monolayers). The reproducibility of the $J-V$ curves from sample to sample is given in the Supporting Information.

TABLE 1: Estimated Total, Organic Monolayer, and Inorganic Thickness

monolayer	total thickness ellipsometry [Å] (±5%)	organic thickness XPS [Å] (±5%)	inorganic thickness XPS [Å] (±5%)
C8	21	12.2	9.1
C10	24		
C12	26	16.9	8.0
C14	28		
C16	30.5		
C18	32.5	25.2	6.8

Units. The x-axis of the $J-V$ curves represents the bias voltage given in volts (V) while the y-axis, which represents the current density, is given in A/cm^{-2}. Potentials are given in V, from which the electron energies in eV can be obtained by multiplying the electron charge q in coulombs.

3. Results and Discussion

Monolayer Properties. ***Ellipsometry.*** One of the major problems in ellipsometry is that the surface roughness generally limits the ability to deduce the absolute thickness of an organic monolayer. Moreover, it is hard to distinguish between different components within the layer when dealing with layers thinner than ∼10 nm. As explained in the Experimental Section, we used a Cauchy "1-layer" model. In ref 29 and its Supporting Information, we showed that using a "2-layer" model for thin layers on GaAs, where the substrate is partly oxidized, yields unreasonably large variations in the widths of the molecular monolayer and of the oxide layer, while their combined width is almost identical to the width deduced with the "1-layer" model. We rechecked this for some samples in the current work and again found no major differences in the total thickness. Therefore, we use the "1-layer" model and deduce the monolayer thickness from XPS measurements. We compare here samples made with alkylphosphonates of different molecular lengths. The measured thickness values are presented in Table 1. We see that increasing the molecular length by two carbons yields the expected increase in thickness (∼2−3 Å for two carbons).

The surface roughness, as determined by atomic force microscopy (AFM) (from a 200× 200 nm area), was found to be 0.6 nm (±0.2 nm). [36]

Contact Angle. The methyl tail groups of the alkyl chain molecules are hydrophobic, and the hydrophobicity of the complete alkyl monolayer will reflect how close these tail groups are packed. Sessile advancing drop contact angle measurements with water can therefore provide a measure of alkyl monolayer packing density. If we assume further that the densest alkyl monolayers are the closest packed layers, the CA provides a measure of alkyl monolayer quality, where quality reflects the extent to which the alkyl molecules cover the substrate with the chains sticking out from the substrate. The importance of these measurements stems from our experience that a small change in contact angle for these films can correspond to a significant change in $J-V$ characteristics.[37] Therefore, in the present work, only samples with contact angle > 110° were used for further experiments. Table 2 gives the measured contact angle for the different monolayers.

FTIR. Fourier transform infrared spectroscopy serves as an additional tool to evaluate the quality of the monolayer. The density of alkyl chains is reflected in the peak position of the antisymmetric stretch of the methylene groups in the chain. As the alkyl chain monolayer changes from a liquid- to a solid-

TABLE 2: Contact Angle and Infrared (IR) Absorption Characterization of Adsorbed Organic Molecular Monolayers

monolayer	contact Angle [deg] (±2°)	IR absorption peak position of the CH_2 antisymmetric stretch [cm^{-1}] (±1 cm^{-1})
C8	112	2921
C10	112	2920
C12	113	2919
C14	113	2919
C16	114	2917
C18	114	2917

like phase, the antisymmetric stretch moves from 2928 to 2917 cm^{-1}.[38] The observed antisymmetric stretch peak positions are reported in Table 2 for the different monolayers (see also figure S4 in the Supporting Information). The frequencies strongly indicate that the monolayer is closely packed with a low density of gauche defects. It is also obvious that denser monolayers are formed as the number of carbons in the alkyl chain increases. This is not surprising since the longer the alkyl chains are, the stronger the (cumulative) *inter*molecular van der Waals interactions between the chains, and thus the energy gain of the system, will be.

XPS. Calculating the [C]/[P] ratio for all samples, while taking into account the photoelectron attenuation corrections, gives values very close to the theoretically expected ones. The P2p peak at 133.9 eV (binding energy—BE) corresponds, as expected, to an oxidized state of the phosphorus.

However, the [O]/[P] ratio is up to three times larger than the expected value. This result reveals the presence of undesired oxygen. The most obvious cause is oxidation of the substrate itself, which is demonstrated clearly by the $Ga2p_{3/2}$ and $As2p_{3/2}$ core level peaks (Figure 2). Those peaks show not only the energies that correspond to the bulk values but also features that are best ascribed to oxidization of these elements. Still, the excess [O] cannot be explained by surface oxidation only, as calculated from the amounts of oxidized Ga and As. In Figure 3 we show that the O1s line is well fitted with two Gaussian—Lorentzian components, at 530.9 and 531.9 eV. The 530.9 eV peak can be attributed to the phosphonate, plus part of the substrate oxide, because this signal is close to the literature values for the binding energy of O in phosphonates and in Ga_2O_3. Furthermore, in terms of elemental concentration, the [O] intensity is roughly 3 times that of [P] plus 1.5 times that of [Ga]. The 531.9 eV peak might be ascribed to a relatively small amount of oxidized As and to O in adsorbed hydroxyl groups, which are not necessarily at the interface. Indeed for longer molecules (C18 compared to C12), the 530.9/531.9 eV intensity ratio decreases, suggesting that the 531.9 eV peak is less interface related than the 530.9 eV one.

XPS-derived thickness values of the organic and the inorganic films on the GaAs (eqs 1 and 2) are given in Table 1. The monolayer thickness (including alkyl chain and phosphonic acid head group), d_{org}, is almost identical to the nominal molecular length (within experimental error), indicating that the molecules are almost perpendicular to the surface (with a tilt angle of at most 15° with respect to the surface normal). In eq 2 the inorganic overlayer can be written as $[Ga^{ox}] + [As^{ox}] + [O^{inorg}]$, where Ga^{ox} and As^{ox} stand for the oxidized signal of the corresponding elements, but because in our case the monolayer is bound to the surface via oxygen, thus making the oxidized substrate part of the electrical pathway, we define the inorganic overlayer as $[O^{inorg}]$. The thickness derived from ellipsometry

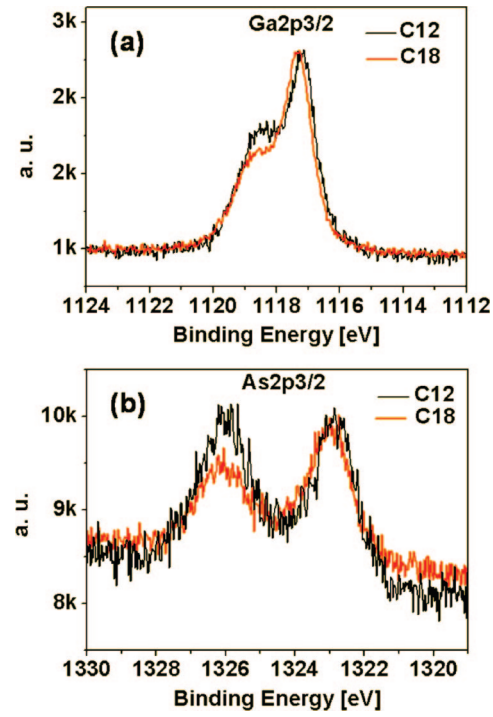

Figure 2. Raw XPS data for a p-GaAs/alkylphosphonate monolayer: (a) the $Ga2p_{3/2}$ region (1117.3 eV peak bulk and 1118.8 eV peak oxide) and (b) the $As2p_{3/2}$ region (1323 eV peak bulk and 1326 eV oxide). Red and black curves are for C18 and C12 monolayers, respectively.

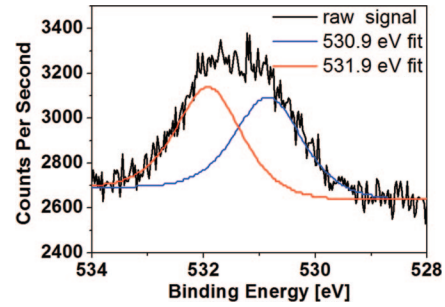

Figure 3. O1s XPS spectral region for p-GaAs/alkylphosphonate C12 monolayer. The peak is best fitted with two Gaussian—Lorentzian components, centered at 530.9 and 531.9 eV.

data, which should add up to ($d_{org} + d_{inorg}$), within some uncertainty due to surface roughness, fits reasonably well with the XPS data.

The overall thickness of the inorganic interface layer (d_{inorg}) shows a slight increase with decreasing monolayer length (Table 1), indicating the improved ability of longer molecules to prevent surface oxidation. The above-mentioned O1s peak ratio for different monolayer lengths is another indication that with increasing monolayer length we find less evidence for interface oxidation.

Because XPS, FTIR, contact angle, and ellipsometry indicate that we have a dense monolayer, we can view the molecular layer as practically continuous and free of holes. For the inorganic layer, though, the thickness values do not necessarily indicate the presence of an additional electrically insulating layer with thickness d_{inorg}. A significant part of the detected oxygen can be incorporated in between the organic molecules, forming a hybrid, and relatively stable, interface, together with the P—O atoms. These *inter*molecular species are thought not to add an additional element in series for the electrical transport measurement.

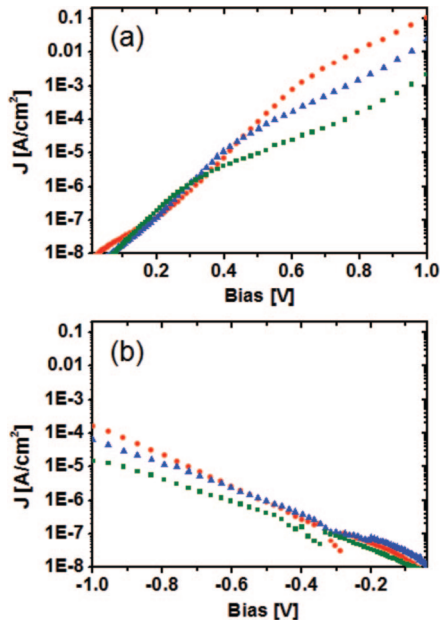

Figure 4. Experimental ln(J)−V curves for n-GaAs/alkylphosphonate monolayer//Hg junctions in the forward (a) and reverse (b) bias regimes: C8, circles; C12, triangles; C18, rectangles. Around 10^{-7} A/cm^2 in the reverse bias the plots are somewhat noisy due to range change of the measuring system.

On the basis of all the measurements presented above, we conclude that these alkyl monolayers on GaAs are of sufficient quality to be studied in metal−insulator−semiconductor (MIS) junctions, with the alkyl chain monolayer as insulator and mercury (Hg) as the metal electrode.

n-GaAs/Molecules/Hg Junctions: $J-V$ Measurements. Figure 4shows the $J-V$ characteristics of n-GaAs/alkylphosphonate/Hg junctions in the reverse and forward bias regimes. We note that there is no detectable change in the $J-V$ characteristics of the samples after repeating the measurements on the same junction. This stability (unlike the case of the unstable GaAs/alkylthiol/Hg junctions[18]) is probably due to the fact that the GaAs−O−P bond is much stronger than the As−S bond. The $J-V$ curves at forward bias show two distinct regimes. At low forward bias (≤0.35 V), all the curves basically coincide. At higher bias, short monolayers pass significantly higher currents than the longer ones. This behavior suggests a switch between electronic transport mechanisms, similar to that observed for alkyl monolayers on Si[15] and in rough agreement with numerical simulations for ideal MIS junctions.[39] We can analyze the $J-V$ data quantitatively, assuming that the currents at negative bias and low forward bias can be described by transport over a barrier in the semiconductor and that, at high forward bias, tunneling through an insulator film starts to participate. Because the barrier in the semiconductor will change with bias, this model also explains the asymmetry of currents at positive and negative bias. Attempts to fit our data using a model, different from direct tunneling, for electronic transport through ultrathin insulators (Fowler−Nordheim tunneling, space charge, or ballistic transport) were unsuccessful, in as far as that no clear correlation with molecular length could be found.

TABLE 3: Electronic Transport Parameters for n- and p-GaAs Alkylphosphonate//Hg Junctions

		C8	C12	C18
n-GaAs	Φ_b, Schottky barrier	0.84±0.02 eV		
	Diode "n" value	1.9±0.2		
	Transition voltage from semiconductor limited - to tunneling-like	~0.61 V	~0.42 V	~0.35 V
	Tunnel barrier and effective mass, Φ_t ; m^*	1.3 ± 0.4 eV;		0.3 ± 0.2m_e
p-GaAs	Tunnel barrier and effective mass, Φ_t ; m^*	0.5 ± 0.2 eV;		0.3 ± 0.2m_e

n-GaAs/Molecules/Hg Junctions: Low Forward Bias Regime. Transport across metal−semiconductor junctions can be described by the thermionic emission−diffusion model[40] (Schottky model)

$$J = A^* T^2 \exp\left(-\frac{q\Phi_b}{kT}\right)\exp\left(\frac{qV}{nkT}\right) \quad (3)$$

where J is the measured current density, A^* is the Richardson coefficient, q is the electron charge, k is the Boltzmann constant, T is the absolute temperature, n is the ideality factor of the junction ($n = 1$ for ideal thermionic emission), and Φ_b is the electrical potential barrier in the space charge region of the semiconductor (also known as the Schottky barrier).[41]

Because the $J-V$ curves of the three types of n-GaAs−alkylphosphonate−Hg junctions at voltages smaller than ~0.35 V are nearly identical, the corresponding ideality factors and Schottky barriers are essentially the same, $n = 1.9 \pm 0.2$ and $\Phi_b = 0.84 \pm 0.02$ eV. The relatively high ideality factor might suggest that another semiconductor-based mechanism is involved (an analysis of which is beyond the scope of this manuscript; a forthcoming publication will consider the mechanisms). Above ~0.35 V the C18 $J-V$ curve no longer falls on the line expected from the TE mechanism. Therefore, we define this point as the transition voltage (for the C18 monolayer) where the TE mechanism no longer dominates and transport via another mechanism (tunneling) becomes significant. We can see that the shorter the monolayers, the higher the transition voltage. We will address this issue when explaining the process in terms of rate-limiting steps in the next section. Table 3 summarizes the basic parameters that can be extracted from analyzing transport across the n-GaAs−alkylphosphonate−Hg junctions at low forward bias within the TE and the direct tunneling (see below) formalisms.

Earlier we showed that only high-quality monolayers exhibit the same TE characteristics for different chain lengths, a phenomenon that was theoretically predicted.[39] We found this behavior to be one of the most sensitive ways to assess monolayer quality.[37] Therefore, the fact that all our n-GaAs junctions show the same $J-V$ characteristic at low forward bias suggests that they are of good quality. This is the first time such a phenomenon is demonstrated in a molecular system where the substrate is not Si.

We found that optimization of the cleaning procedure, after molecule absorption, is crucial to get this type of low-forward-bias $I-V$ behavior. On one hand, cleaning with mild solvents or at room temperature leaves some physisorbed material on top of the monolayer, which can be detected by ellipsometry and deduced from the $J-V$ characteristics. On the other hand, excessive cleaning with physical agents (swabs, etc.), as we used previously, [14] might cause damage to the monolayer. The fact

that the "telltale" low-forward-bias (TE) behavior was not observed in the past is probably related to this delicate balance in cleaning, since all other preparation conditions were identical.

n-GaAs/Molecules/Hg Junctions: Tunneling Analysis—High-Bias Regime. In the forward high-bias regime (>∼0.8 V) the band bending is sufficiently reduced that tunneling across the molecular insulator becomes the main transport-limiting process. We can then analyze the data in that regime using, as a first approximation, the simple linearized version of the Simmons model[42,43] for tunneling through a rectangular barrier (forthcoming publications will compare this analysis with more advanced approaches to modeling).

In this model, which is derived from the Wentzel−Kramers−Brillouin (WKB) approximation for tunneling through an insulator, the transmission probability through the barrier depends exponentially on d, the tunneling distance, and on the attenuation factor β

$$J = J_0 \exp(-\beta d) \tag{4}$$

where β depends on the applied bias

$$\beta = 2\sqrt{\frac{2m^*\left(\Phi_t - \frac{qV}{2}\right)}{\hbar^2}} \tag{5}$$

Here m^* is the effective mass of the electron for the tunneling process, h is Planck's constant, and Φ_t is the tunneling barrier.

From the slope and the intercept of a plot of β^2 vs V (using d_{org} for thickness), we deduce a tunneling barrier $\Phi_t = 1.3 \pm 0.4$ eV and an effective mass $m^* = 0.3 \pm 0.2m_e$, where m_e is the free electron mass. The values have large error margins because of the multiple steps needed to extract them. In addition, we note that these values come from a greatly simplified model, which does not take into account the barrier shape and the asymmetry of the junction.

The extent to which the use of a more involved version of the linearized version of the Simmons model can improve significantly our ability to analyze these and similar data is being studied separately and will be discussed for this and other junctions in a future report.

n-GaAs/Molecules/Hg Junctions: Rate-Limiting Step. One of the most striking features of electronic transport across these molecular MIS junctions is the competition between different transport mechanisms. To check the role of tunneling in the low-forward-bias regime, we consider as a test case the longest monolayer (n-GaAs−O_3P−C18/Hg junction), where tunneling is most likely to play a role in transport.

Since the electrons that cross the junction need to overcome the Schottky barrier in the semiconductor and also cross the organic molecule, we view transport through these two adjacent spatial regions as two coupled processes in series. As a first approximation we treat the characteristic currents, J_{sc} and J_{ml}, as emission over a barrier in the semiconductor and tunneling across the monolayer. In this view we can treat these currents as reaction rate constants (i.e., k_{sc} and k_{ml}), where the reaction is electron transport from one side of the junction to the other side and the individual (TE and tunneling) currents are the rates. We can then write the overall reaction for such a process[18] as

$$A \xrightarrow{k_{sc}} A^* \xrightarrow{k_{ml}} B \tag{6}$$

If $k_{sc}/k_{ml} \ll 1$, the rate of charge transport through the semiconductor, J_{sc}, will control the transport. If $k_{sc}/k_{ml} \gg 1$, the rate of charge transport through the insulating layer, J_{ml}, will dominate. But, if k_{sc} and k_{ml} are comparable, the measured current will, to a significant extent, be limited by both rates. As a characteristic measure for the semiconductor-limited current, we define $J(0)$, the extrapolated current at 0 V, derived from the ln(J) vs V plots, shown in Figure 4, while the characteristic tunneling-limited current through the monolayer is proportional to $\exp(-\beta(0)d)$. In the case of the n-GaAs−O3P−C18/Hg junction, the analysis of the experimental $J-V$ curves shows

$$\frac{J_{sc}}{J_{ml}}\left(\propto \frac{J(0)}{\exp(-\beta(0)d)}\right) \cong 0.05 \tag{7}$$

Because $J_{sc}/J_{ml} \ll 1$, the current transport is controlled by the Schottky barrier even for the thickest monolayer in the low-bias regime, an interpretation supported by previous findings.[44] In that work, we showed temperature-dependent $J-V$ measurements on junctions made with these alkylphosphonate monolayers on GaAs. In the low-bias regime (for n-GaAs), the current was found to increase with increasing temperature, as expected for a semiconductor-barrier-limited dominant mechanism. In the high-forward-bias regime, no significant change in current was observed with change in temperature, in agreement with transport dominated by tunneling.

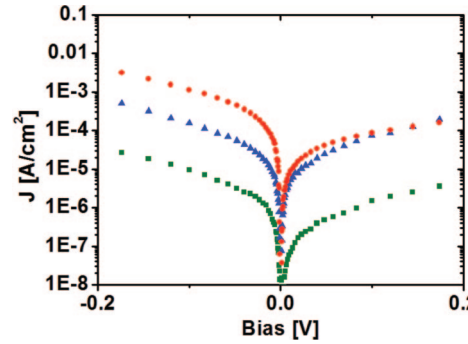

Figure 5. Experimental ln(J)−V curves for p-GaAs/alkylphosphonate monolayer//Hg junctions in the forward and reverse bias regimes: C8, circles; C12, triangles; C18, rectangles.

p-GaAs/Molecules/Hg Junctions. An important difference between a semiconductor/molecule and metal/molecule system is that a change in dopant type or density changes the Fermi level position within the semiconductor band gap. This property provides another opportunity to understand transport behavior, because it allows changing the energetics of the system without, in first approximation, affecting the nature of the chemical bond. Therefore, we studied the same alkyl chains also on p-GaAs. No significant difference in monolayer properties is observed between n- and p-GaAs, as seen by ellipsometry, contact angle, and XPS measurements.

p-GaAs/Molecules/Hg Junctions: $J-V$ Measurements. The $J-V$ curves for the p-GaAs/alkyl/Hg junctions are shown in Figure 5. Characteristics at positive and negative bias are less asymmetric than with n-GaAs, with a pronounced dependence on the length of the alkyl chains at both polarities, contrary to the results found with n-GaAs.

Using eq 7 we find $J_{sc}/J_{ml} \gg 1$ for all the monolayers, which shows that the bottleneck for transport is the monolayer and the limiting mechanism is tunneling. Attempts to analyze our data with other electronic transport mechanisms (Fowler−Nordheim tunneling, space charge, and ballistic transport) showed poor fits and no correlation with molecular length.

The $J-V$ curve is most sensitive to monolayer quality if the semiconductor barrier dominates transport (cf. ref 36). From Figure 5 we can deduce from the residual asymmetry of the curves that at positive bias range the semiconductor barrier

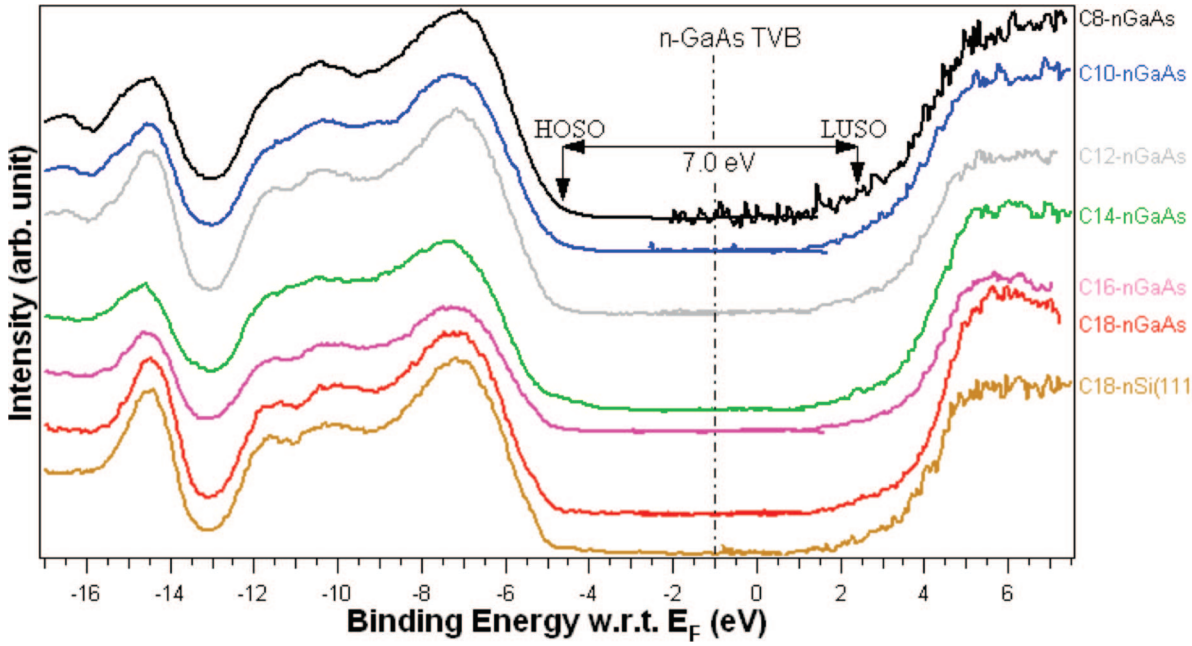

Figure 6. Combined UPS and IPES spectra for the n-GaAs/alkylphosphonate interfaces. The UPS and IPES spectra of the n-Si (111)/C18H37 interface[50] are shown for comparison. The vertical dashed-dotted line at −1 eV represents the position of top of the valence band of the substrate.

enters, albeit a relatively small one. It appears, therefore, that the C12 monolayer is of lesser quality than the C8 and C18 ones, something that is not expressed in the "normal" characterizations but can be seen in the transport.

Using the linearized version of the simple Simmons model (eq 4) and the procedure outlined above, the tunneling barrier and effective mass are found to be $\Phi_t = 0.5 \pm 0.2$ eV and $m^* = 0.3 \pm 0\ 0.2m_e$, respectively (using d_{org} for thickness).

Even though, as we explained above, the inorganic layer is not considered to be an additional resistance layer, we note that also if we use ($d_{org} + d_{inorg}$) as barrier width in these calculations, this results in only minor changes: $\Phi_t = 1.1 \pm 0.4$ eV and $m^* = 0.3 \pm 0\ 0.2m_e$ for n-GaAs and $\Phi_t = 0.5 \pm 0.2$ eV and $m^* = 0.4 \pm 0\ 0.2m_e$ for p-GaAs junctions.

UPS and IPES Measurements. In order to determine energy level positions and interface charge injection barriers, we performed UPS and IPES[45] measurements on the monolayer/GaAs systems, i.e., without top contact. UPS and IPES data collected for different lengths of molecules chemisorbed on n-GaAs are shown in Figure 6. The latter shows He II spectra of a series of alkyl chains on GaAs. On the graph, the *x*-axis represents the binding energy with respect to the Fermi level (E_F). The electronic structure of these alkyl chains are analogous to the data previously recorded on Si(111)[46] (cf. bottom curve of Figure 6). This demonstrates that the UPS and IPES signal from the alkylphosphonate/GaAs junction is dominated by the signal from the saturated chains themselves. We note that adding the top contact (Hg in the present case) changes the electronic structure of the system,[47] in particular the band bending in the semiconductor. This is clear from that only 0.3−0.4 eV band bending is found from SPV measurements on monolayer/n-GaAs samples *without a top contact*, while we find a 0.84 eV Schottky barrier from *J*−*V* measurements on junctions *with a top Hg electrode* (see Supporting Information for determining band bending by XPS and UPS). However, since the molecules are attached chemically to the GaAs surface and only physically to the Hg electrode, much of the electronic nature of the junction, i.e., the position of the molecular levels relative to the semiconductor band edges, is captured by UPS and IPES measurements on the free alkyl/GaAs surface. As we have learned from previous systems, UPS and IPES measure the composite semiconductor/molecule interface states, which we will call here highest occupied system orbitals (HOSO) and lowest unoccupied system orbitals (LUSO).

As explained in the Supporting Information, we can now use these data, the corresponding XPS data from core levels (taken both at WIS and PU), and the results from computations performed on alkyl/Si by Segev et al.,[46] which provide a good approximation of the molecular levels of the alkyl chains, to build energy diagrams, including GaAs band bending, of the semiconductor/molecule/(metal) systems. Figure 7b shows the energy diagram for the n-GaAs-alkylphosphonate/Hg system. The GaAs band gap is 1.4 eV. For the doping densities of our n-GaAs samples, the Fermi level in the bulk is essentially at the bottom of the conduction band. The HOSO position, taken as the highest energy onset of the UPS spectrum, is 4.6 ± 0.2 eV below the Fermi level (Figure 7a). From IPES we find the LUSO, taken as the low-energy onset of the spectrum, to be 2.4 ± 0.2 eV above the Fermi level. This yields a HOSO−LUSO gap of approximately 7.0 eV. This value is close to the gap found for alkyl monolayers bound to Si as well as for thick alkane films.[48] The reason for the discrepancy with our earlier analysis of the GaAs−alkylthiols spectra[18] is given in the Supporting Information. We note that the HOMO−LUMO gap of the free alkyl chain in gas phase is ∼9−10 eV. The reduction of the gap observed in the case of the condensed phase is mainly due to some polarization effect. This phenomenon is due to the electronic polarization induced by the alkyl cation and anion that appear at the interface during the direct and inverse photoemission process.[49]

Figure 8b shows the proposed band diagram for the p-GaAs/alkylphosphonate//Hg system. For the doping densities of our p-GaAs samples, the Fermi level in the bulk is essentially at the top of the valence band. The HOSO−LUSO gap is unchanged in comparison to the n-GaAs-alkylphosphonate system (Figure 8a). From IPES we find the LUSO near the GaAs

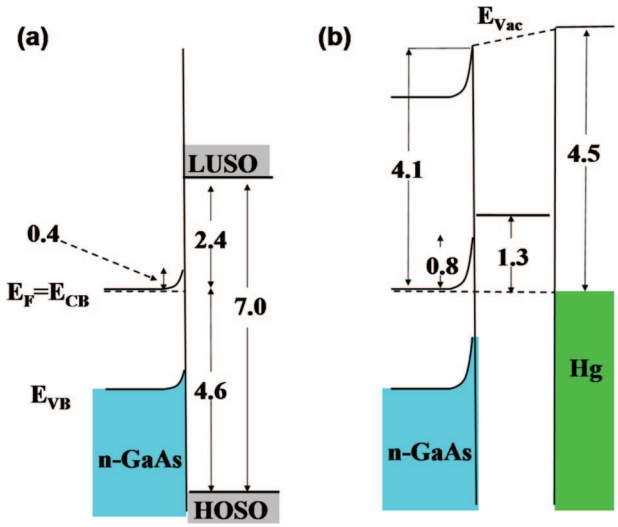

Figure 7. (a) Proposed band diagram for n-GaAs/alkylphosphonate monolayer interface, where the HOSO and LUSO values were determined by UPS and IPES, respectively, and the band bending was deduced from SPV measurements. (b) Proposed energy band and level diagram for the n-GaAs/ alkylphosphonate monolayer//Hg junctions. The Schottky ($\Phi_b = 0.84 \pm 0.02$ eV) and tunneling barriers ($\Phi_t = 1.3 \pm 0.4$ eV) are determined from analyzing current transport data.

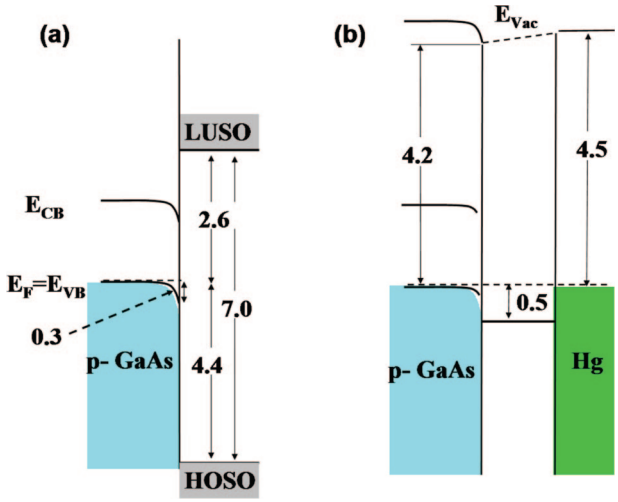

Figure 8. (a) Proposed band diagram for the n-GaAs/alkylphosphonate monolayer interface, where the HOSO and LUSO values were determined by UPS and IPES, respectively, and the band bending was deduced from SPV measurements. (b) Proposed band diagram for the p-GaAs/alkylphosphonate monolayer//Hg junctions. The tunneling barrier ($\Phi_t = 0.5 \pm 0.2$ eV) was determined from analyzing the current transport data.

conduction band minimum and a large density of states at 2.6 ± 0.2 eV above the Fermi level. UPS gives for the HOSO 4.4 ± 0.2 eV below the Fermi level (see also figure S5 in the Supporting Information).

What is "the Real Tunneling Barrier"? While the $J-V$ measurements on the n-GaAs junctions show a 1.3 eV tunneling barrier, from UPS we expect a 2.4 eV tunneling barrier based on the LUSO (Figure 7a). It is thus obvious that a direct conversion from the energy diagram of the semiconductor cum molecules system (Figures 7a and 8a) to the energy band/level diagram of the metal−molecules−semiconductor system (Figures 7b and 8b) (and vice versa) is not straightforward. This discrepancy can be understood if we invoke the induced density of interface states (IDIS) model, which we proposed earlier to be valid for the Si-alkyl system,[50] also based on DFT electronic structure calculations.[46] Interactions of the wave functions of the semiconductor substrate (GaAs, in our case) and the metallic electrode (Hg, in our case) with those of the alkyl chain molecules IDIS. From IPES and UPS experiments, we find approximate energies of the HOSO and LUSO states, based on the highest density of states closest to the Fermi level. These values are important as they present upper limits and also allow comparison between different molecular systems. HOWEVER, there are states (of lower density) that are closer to the Fermi level and, hence, contribute and can even dominate the charge transport. These interface states have energies inside the molecular monolayer gap and can extend to the semiconductor band edges, as was found to be the case for the Si system, using very high resolution UPS.[46] In this picture, charge transport is best described by an ensemble of tunneling paths at each of the energies between the semiconductor and molecular monolayer band edges/orbital energies. Each path then has a tunnel barrier energy according to the specific energy of the IDIS, with an added probability factor that is related to the density of states at that specific energy. Because the tunneling model uses one barrier only (this holds also for more sophisticated models), analysis of the $J-V$ measurements can yield only one barrier value, which, therefore, should be viewed as an *effective barrier* rather than as "the real one". In that sense, the effective value represents a weighted average of many different barriers.

4. Conclusions

From charge transport measurements, we find that for n-GaAs samples at low forward bias the results can be interpreted in terms of semiconductor-limited transport. Especially the coinciding of the characteristics for molecules of different lengths strongly points to this mechanism, as well as to the high-quality of the monolayers. p-GaAs data at all forward bias voltages, and those at high forward bias for n-GaAs, are interpreted in terms of direct tunneling through an insulator, the organic molecular layer. Analyzing those data with the simple, linearized Simmons model, modified for use with organics, a model that has tunnel barrier height, length, and electron effective mass as parameters, and using ellipsometry and XPS-derived organic layer width data, yields values for a tunneling barrier and carrier effective mass. We show discrepancies between the tunneling barriers deduced from $J-V$ measurements and those obtained from UPS and IPES. This discrepancy is attributed to the distribution of gap states and their energy-dependent contribution to the charge transport. Thus, the barrier derived from $J-V$ measurements is an effective barrier.

Acknowledgment. We thank L. Kronik, A. Salomon, and L. Segev for fruitful discussions. The work in WIS is partially supported by the Israel Science Foundation (ISF), the Minerva Foundation (Munich), the U.S.−Israel Binational Science Foundation (Jerusalem), the NATO Science for Peace Program, and research grants from Mr. and Mrs. Jay Bycer and from 21 Ventures. H.S. holds an ISF convergent technology predoctoral fellowship. D.C. holds the Rowland and Sylvia Schaefer Chair in Energy Research. The work at Princeton University was supported by the NSF (DMR-0705920) and the Princeton MRSEC of the NSF (DMR-0213706).

Supporting Information Available: This material is available free of charge via the Internet at http://pubs.acs.org.

References and Notes

(1) Seker, S.; Meeker, K.; Kuech, T. F.; Ellis, A. B. *Chem. Rev.* **2000**, *100*, 2505.

(2) Ashkenasy, G.; Cahen, D.; Cohen, R.; Shanzer, A.; Vilan, A. *Acc. Chem. Res.* **2002**, *35*, 121.
(3) Green, A. M.; Spicer, W. E. *J. Vac. Sci. Technol., A* **1993**, *11*, 1061.
(4) Ohno, H.; Chiba, D.; Matsukura, F.; Omiya, T.; Abe, E.; Dietl, T.; Ohno, Y.; Ohtani, K. *Nature* **2000**, *408*, 944.
(5) Malajovich, I.; Kikkawa, J. M.; Awschalom, D. D.; Berry, J. J.; Samarth, N. *J. Appl. Phys.* **2000**, *87*, 5073.
(6) Wu, D. G.; Ashkenasy, G.; Shvarts, D.; Ussyshkin, R. V.; Naaman, R.; Shanzer, A.; Cahen, D. *Angew. Chem., Int. Ed.* **2000**, *39*, 4496.
(7) Sheen, C. W.; Shi, J.-X.; Mairtensson, J.; Parikh, A. N.; Allara, D. L. *J. Am. Chem. Soc.* **1992**, *114*, 1514.
(8) Hsu, J. W. P.; Lang, D. V.; West, K. W.; Loo, Y. L.; Halls, M. D.; Raghavachari, K. *J. Phys.Chem. B* **2005**, *109*, 5719.
(9) McGuiness, C. L.; Shaporenko, A.; Zharnikov, M.; Walker, A. V.; Allara, D. L. *J. Phys. Chem. C* **2007**, *111*, 4226.
(10) Aqua, T.; Cohen, H.; Vilan, A.; Naaman, R. *J. Phys. Chem. C* **2007**, *111*, 16313.
(11) Ohno, H.; Nagahara, L. A.; Mizutani, W.; Takagi, J.; Tokumoto, H. *Jpn. J. Appl., Phys. Part 1* **1999**, *38*, 180.
(12) Vilan, A.; Ussyshkin, R.; Gartsman, K.; Cahen, D.; Naaman, R.; Shanzer, A. *J. Phys. Chem.* **1998**, *102*, 3307.
(13) Artzi, R.; Daube, S. S.; Cohen, H.; Naaman, R. *Langmuir* **2003**, *19*, 7392.
(14) Nesher, G.; Shpaisman, H.; Cahen, D. *J. Am. Chem. Soc.* **2007**, *129*, 734.
(15) Salomon, A.; Boecking, T.; Chan, C. K.; Amy, F.; Girshevitz, O.; Cahen, D.; Kahn, A. *Phys. Rev. Lett.* **2005**, 95.
(16) Thieblemont, F.; Seitz, O.; vilan, A.; Cohen, H.; Salomon, E.; Kahn, A.; Cahen, D. *Adv. Mater.*, in press.
(17) Lodha, S.; Janes, D. B. *Appl. Phys. Lett.* **2004**, *85*, 2809.
(18) Nesher, G.; Vilan, A.; Cohen, H.; Cahen, D.; Amy, F.; Chan, C.; Hwang, J. H.; Kahn, A. *J. Phys. Chem. B* **2006**, *110*, 14363.
(19) Vilan, A.; Shanzer, A.; Cahen, D. *Nature* **2000**, *404*, 166.
(20) Hipps, K. W. *Science* **2001**, *294*, 536.
(21) Vilan, A.; Pejoux, C.; Cahen, D. *Adv. Funct. Mater.* **2002**, *12*, 795.
(22) Loo, Y. L.; Lang, D. V.; Rogers, J. A.; Hsu, J. W. P. *Nano Lett.* **2003**, *7*, 913.
(23) Haick, H.; Ambrico, M.; Ghabboun, J.; Ligonzo, T.; Cahen, D. *Phys. Chem. Chem. Phys.* **2004**, *6*, 4538.
(24) Slowinski, K.; Fong, H. K. Y.; Majda, M. *J. Am. Chem. Soc.* **1999**, *121*, 7257.
(25) Holmlin, R. E.; Haag, R.; Chabinyc, M. L.; Ismagilov, R. F.; Cohen, A.; Terfort, A.; Rampi, M. A.; Whitesides, G. M. *J. Am. Chem. Soc.* **2001**, *123*, 5075.
(26) Selzer, Y.; Salomon, A.; Cahen, D. *J. Am. Chem. Soc.* **2002**, *124*, 2886.
(27) Vilar, M. R.; El Beghdadi, J.; Debontridder, F.; Artzi, R.; Naaman, R.; Ferraria, A. M.; do Rego, A. M. B. *Surf. Interface Anal.* **2005**, *37*, 673.
(28) Adlkofer, K.; Tanaka, M. *Langmuir* **2001**, *17*, 4267.
(29) Vilan, A.; Ghabboun, J.; Cahen, D. *J. Phys. Chem. B* **2003**, *107*, 6360.
(30) Cohen, R.; Kronik, L.; Shanzer, A.; Cahen, D.; Liu, A.; Rosenwaks, Y.; Lorenz, J.; Ellis, A. B. *J. Am. Chem. Soc.* **1999**, *121*, 10545.
(31) Wen, K.; Maoz, R.; Cohen, H.; Sagiv, J.; Gibaud, A.; Desert, A.; Ocko, B. M. *ACS Nano* **2008**, *2*, 579.
(32) Cumpson, P. J.; Seah, M. P. *Surf. Interface Anal.* **1997**, *25*, 430.
(33) Briggs, D.; Seah, M. P. *Practical surface analysis*; Wiley: New York, 1990; Vol. 1.
(34) Recep, A.; Qing, C.; Gerald, J. L. *Rev. Sci. Instrum.* **1989**, *60*, 3643.
(35) Wu, C. I.; Hirose, Y.; Sirringhaus, H.; Kahn, A. *Chem. Phys. Lett.* **1997**, *272*, 43.
(36) Adding a surface roughness model to the Cauchy model (using the AFM roughness as input) could improve the accuracy of the total thickness, deduced from ellipsometry.
(37) Seitz, O.; Bocking, T.; Salomon, A.; Gooding, J. J.; Cahen, D. *Langmuir* **2006**, *22*, 6915.
(38) Allara, D. L.; Nuzzo, R. G. *Langmuir* **1985**, *1*, 52.
(39) Shewchun, J.; Green, M. A.; King, F. D. *Solid-State Electron.* **1974**, *17*, 563.
(40) Sze, S. M. *Physics of Semiconductor Devices*, 2nd ed.; Wiley: New York, 1981.
(41) Current transport mechanisms, different from thermionic emission, can be formulated with the same functional current−voltage dependence, e.g., diffusion/recombination for an abrupt p^+/n junction, but with a different pre-exponential factor and temperature dependence. In a forthcoming publication, we will discuss the issue of different semiconductor-limited transport mechanisms in metal/molecules/semiconductor systems.
(42) Simmons, J. G. *J. Appl. Phys.* **1963**, *34*, 2581.
(43) Simmons, J. G. *J. Appl. Phys.* **1964**, *35*, 2655.
(44) Salomon, A.; Shpaisman, H.; Seitz, O.; Boecking, T.; Cahen, D. *J. Phys. Chem. C* **2008**, *112*, 3969; see figure SI-2.
(45) Cahen, D.; Kahn, A. *Adv. Mater.* **2003**, *14*, 271.
(46) Segev, L.; Salomon, A.; Natan, A.; Cahen, D.; Kronik, L.; Amy, F.; Chan, C. K.; Kahn, A. *Phys. Rev. B* **2006**, *74*, 165353/1.
(47) Tung, R. T. *Phys. Rev. Lett.* **1984**, *52*, 461.
(48) Delhalle, J.; Andre, J. M.; Delhalle, S.; Pireaux, J. J.; Caudano, R.; Verbist, J. J. *J. Chem. Phys.* **1974**, *60*, 595.
(49) Amy, F.; Chan, C.; Kahn, A. *Org. Electron.* **2005**, *6*, 85.
(50) Salomon, A.; Boecking, T.; Seitz, O.; Markus, T.; Amy, F.; Chan, C. K.; Cahen, D.; Kahn, A. *Adv. Mater.* **2007**, *19*, 445.

JP808086D